Traceability of acoustic emission measurements for micro and macro grinding phenomena—characteristics and identification through classification of micro mechanics with regression to burn using signal analysis

Griffin, JM

Traceability of Acoustic Emission measurements for micro and macro grinding phenomena – Characteristics and Identification through classification of micro mechanics with regression to burn using signal analysis

Abstract: During the unit event of material interaction in grinding three phenomena are involved namely: rubbing, ploughing and cutting. Where ploughing and rubbing essentially mean the energy is being applied less efficiently in terms of material removal. Such phenomenon usually occurs before or after cutting. Based on this distinction it is important to identify the effects of these different phenomena experienced during grinding. Acoustic Emission (AE) of the material grit interaction is considered the most sensitive monitoring process to investigate such miniscule material interactions. For this reason two AE sensors were used to pick up energy signatures (one verifying the other) correlated to material measurements of the horizontal scratch groove profiles. Such material measurements would display both the material plastic deformation and material, removal mechanisms. Previous work has only partially displayed the link in terms of micro and macro phenomena (unit event to normal MG events). In the work presented here, the micro unit grit event will be linked to the macro phenomena such as: normal grinding conditions extended to aggressive conditions: burn. This is significant to any safety critical manufacturing environment due to burn providing surfaces that cannot be accepted when scrutinised under quality considerations and therefore plays an integral part into abrasive machining process. This paper also looks at transparent classification: CART to give regression capabilities in displaying the micro to macro phenomena in terms of signal intensities and frequency representation.

The demarcation between each of the phenomenon was identified from acoustic emission (AE) signals being converted to the frequency-time domains using Short Time Fourier Transforms (STFT).

1. **Introduction**

Material particle displacements can be observed from the emitted elastic waves that propagate through material media [1] when an object is subjected to an external force in terms of an initiated material stress. The released energy is primarily in the form of Acoustic Emission (AE). From various stresses there are material particle displacements which are associated with AE and released in the form of material elastic energy. These elastic AE waves mimic the mechanical vibration of material and grit interaction and are extracted by AE sensors. Different AE characteristic signals are analogous to different external forces that act on the same material or the same force exerted on different materials [2-4]. Elastic waves can therefore be used for monitoring many machining processes and/or material non-destructive tests [5-8].

AE monitoring may be a difficult task; however with correct data it is possible to monitor grinding phenomena features of interest. In this paper there is a focus on identifying the different levels of cutting phenomenon and what such levels can mean in standard grinding and that of abusive grinding conditions such as burn. It can be said that varying levels of SG interaction is an easier phenomenon to observe when

compared to that of grinding. This is in terms of the distinguishing features between cutting, ploughing and rubbing and the irregular distribution of grains when interacting with the material workpiece. Once the observations and associated data have been achieved to distinguish between different features it can then be used to look at different levels of cutting, ploughing and rubbing experienced during the macro normal grinding event. There has been a lot of work on SG analysis previous to this work where the material removal mechanisms were investigated from microscopic analysis and acquired force signals [9-10]. However, there has been no work to date linking the micro to the macro event through the use of extracted AE signals. Traditionally AE analysis used Root-Mean-Squared (RMS) level detection, event count, and energy distributions, amplitude and the powers of dominate frequency bands [4]. To date, little work has investigated energy relationships experienced during SG scratch tests compared to actual grinding tests using continuous, high fidelity AE analysis [2-3].

The research presented here looks at the identification of micro grinding phenomena with grinding/burn. Grinding burn can be considered as a key unwanted phenomenon when grinding aerospace materials such as CMSX4 [11]. This is due to the uneven re-hardening of a material giving brittle characteristics as well as the increased possibility of micro cracks [8]. If burn or even slight burn occurs during the manufacturing process of critical parts (turbine blade or disk), then that unit may have to be scrapped. This action is due to the aerospace requirements being very stringent when manufacturing commercial safety critical parts. For instance, if they fail due to a hair line crack caused by slight burn [2][11] this could cause catastrophic results and ultimately result in death [12].

Moreover, grinding burn occurs from the increased grinding temperature when abrasive grits come into contact with workpiece material. This temperature however, cannot dissipate quickly due to too much heat generated during material being removed or, not enough coolant present suppressing friction. There are other factors such as a worn grinding wheel due to the loading effect where such mechanisms such as ploughing and rubbing are more dominant. This burn has to be monitored in such a manner to promote the pre-emptive action. For instance, during trials there were high RMS amplitudes for the start and end of the cutting process, which could be confused with the phenomenon of interest. There is a need therefore to understand micro and macro mechanisms to identify the onset of anomalies and promote less misclassification, false alarms. The following research looks at applications of AE monitoring which can be applied to the proposed work. Tonshoff et al. [13] discusses the possibility to link AE waveforms to the surface roughness through the use of a Taylor Hobson Talysurf precision measuring device. The research discussed by Chen et al. [14-15] looks at the extraction and identification of grinding burn through AE signals. They used both Wavelet Packet Transforms (WPT) and Short Time Fourier Transforms (STFT) to identify phenomena of interest. Both sets of investigations display how the micro can be connected to the macro event.

In this paper, the research looks at the results gained from two trials, SG tests and grinding tests significant of the burn phenomenon (using the same machine feed rates, wheel velocities and materials). The investigation presented here investigated Short-Time Fourier Transforms (STFT) to convert the raw extracted AE time series signal into time based frequency signal, segmented into different frequency bands. The AE

signals were verified with force, power signals, roughness measurements, and observations.

Machine learning techniques have played a vital role in assisting machine process monitoring. Of the many techniques applied to monitoring, Neural Networks (NN) are considered the most extensive however, in the last decade a number of different classifiers with a greater emphasis towards evolutionary and rule-based computing techniques have emerged as successors to this type of classifier. NN functions are considered as black box classifiers in that it is difficult to understand which patterns are more significant than others. With classification and regression trees (CART) there is a lot more transparency and they are particularly useful for correlating micro with macro phenomena. In addition, CART is useful in discriminating large data sets which is often associated to the majority of classifier inaccuracies.

Research using fuzzy neural networks investigates it is possible to quantify overlapping wear states through AE signals during micro milling which suggests the sensitivity of AE used to distinguish microscopic phenomena [16]. Ren et al. investigate the same machining process where fuzzy identification using extended subtractive cluster analysis and least squares allows the accurate measure of material removal mechanisms [17]. The research discussed in this paper uses similar ideas in identifying microscopic features achieved during single grit (SG) grinding scratch and macro, normal grinding tests. Moreover, the precision of AE technologies applied to wear can be directly related to material removal mechanisms achieved during SG scratch and macro grinding tests. By using fuzzy clustering or methods very similar such as CART it is possible to link SG and multiple grit (MG) grinding phenomena.

The main investigation objectives of this paper are:

• Characterise cutting, ploughing and rubbing phenomena in horizontal SG scratch tests using material profile measurement techniques correlated to AE signal event.

• Analyse cutting, ploughing and rubbing signals for SG interaction of CMSX4 and Titanium-64, aerospace materials.

• Compare SG with grinding signals of both CMSX4 and Titanium-64 aerospace materials.

• Compare SG with grinding signals of both CMSX4 and Titanium-64 burn phenomena.

• Correlate SG with MG AE grinding phenomena using statistical parallel co-ordinates.

• Classification using CART to correlate the micro with the macro grinding event.

• To confirm significant frequency domains between SG and the macro event parallel-coordinates were used.

The investigations of SG horizontal scratch work in extracting AE waveforms to identify the energy footprints of cutting, ploughing and rubbing during conventional grinding is both novel and provides a different focus in obtaining efficient cutting conditions especially when correlated to the macro grinding phenomena event. The rest of the paper is organised into the following sections: (2) Acoustic Emission Technology (3) Experimental Setup, (4) Acoustic Emission with force signals, (5) Transparent Classification Technologies, (6) Classification Results (7) Discussion of Results (8) Conclusions.

2. Acoustic Emission Technology

The sensitivity of AE sensors is of paramount importance to identify the onset of plastic deformation, for example; when applied to SG tests the AE phenomenon is so minuet and localized it is difficult to detect and thus there is a need for sensitivity. AE generated from material under stress refers to the generation of transient elastic waves during the rapid release of energy from the localized sources within a material. The difference between the AE technique and other non-destructive evaluation (NDE) methods is that AE detects the activities inside the materials, while other NDE methods attempt to examine the internal structures of the materials. Furthermore, AE only needs the input of one or more relatively small sensors fixed to the surface of the structure or specimen under examination.

The disadvantage of AE is that commercial AE systems can only estimate qualitatively how much damage is in the material and approximately how long the components will last. So, other NDE methods are still needed to do more thorough examinations and provide quantitative results (such as force and displacement sensors).

2.1   AE Calibration and reliability of signal analysis

AE is seeing more applications used in industry due to the possibilities to measure a change in minute phenomena however calibration methods for such developing technologies have not been accepted in terms of standardisation and instead are only associated with best practices [18].

Hatano et al. [19] looked at pencil calibrations to investigate the AE elastic wave time/velocity and phase behaviour. Also summarised in [19] spurious waves do not

make a huge significance to dominant waves (Raleigh and longitudinal). In short, the AE elastic waves are located in terms of the dominant energy bands which is fundamental to the work presented here. Pencil calibrations are used to give an AE reference level for different tests carried out at different times, however care must be taken with respect to material size and distances measured from the sensors. For example, it was noticed that the burn tests carried in [2] and the work carried out here have different levels where the materials were very similar (exotic aerospace materials). Nevertheless the differences between normal grinding and burn is roughly three times which relate to similar patterns discussed here (the appreciation is in regard to relative calibrated patterns). The difference being is the microphones were nearer to the workpiece when compared with the work discussed in [2]. Care needs to be taken when considering sensor distances and extracted energies [3] and noted. In terms of using AE as source for comparison, the microphones were set up the same for the SG and grinding tests (the 2 AE sensors were set on level plains across from each other). The additional force sensor acts as arbitrator for reference to an absolute standardised source.

2.2   AE used with classifier technologies

Goding et al. [20] looks at using k-means and self-organising maps (SOM) which are similar to fuzzy-neural classifiers in segregating different mechanisms of material failure under tensile tests with recorded AE signals. Where such AE is reduced in terms of n-dimensionality to give the rise time, peaks and, the counts of the threshold passes. CART technologies are considered similar in functionality to fuzzy classifier technologies [21].

3. Experimental Setup for AE calibration tests

There were two experiments carried out for this work, the first consisted of SG tests significant of prolonged emitted stress for two aerospace materials (See Figure 1) for setup. The second looked at various AE emitted sources significant of grinding and grinding burn (see Figure 2).

Figures 1 and 2 display the set-up for the micro SG and macro grinding experiments respectively.

Figure 1 Single Grit Experimental setup

By setting up the experiment displayed in Figure 2 and providing increasing depth of cuts it was possible to gain burn phenomenon with increasing intensities. The burn phenomenon would then be recorded by an AE sensor, force dynamometer, accelerometer, power meter and a record of workpiece/grinding wheel image. The phenomenon would be measured in terms of where it occurred on the workpeice.

Figure 2 A55 Machine Centre Set-up for Burn Experiment (CMSX4)

The grinding cut signal obtained by each sensor would then be stripped from the total recorded stream and measured to correlate the physical burn source with the digitised signal source. This is fundamental to the understanding of different grinding phenomena.

As shown in Figure 2, the set-up of the grinding process monitoring consisted of the following: A Makino A55 machine centre, two Digital Acquisition Cards (DACs) being housed on separate computers, a Kistler Dynamometer and accelerometer measurement system was situated next to the workpeice to take full advantage of material vibrations. The AE sensors (PAC wideband sensors) were cased in purpose built sensor housing facilities to protect them from the harsh grinding environment. The continuous waveform format provides all the required information and this was used instead of event driven methods. Both Chebyshev Type II low and high pass filters were used to remove any mechanical or any white noise past 1.2 MHz range.

3.1   Burn tests

For the burn trials the machine was set-up with a fixed workpiece and grinding wheel attached to the spindle (see Figure 2). The AE sensor system would be calibrated by a 2H, 0.5 mm automatic pencil [18] for all tests. Grinding conditions were adjusted as required for the experiment (in the burn case increasing depth of cut with no coolant in order to gain burn and more intense burn characteristics for Titanium however coolant was necessary due to the combustible nature of the material, especially at 1 mm DOC). The extracted signals would then be logged and saved to files. The sample width and thickness would be measured and noted along with observations of the temper colour change signifying the physical burn characteristics (25x-50x magification). These steps would be repeated for successive depth cuts and the measurement of the wheel diameter at the end of the trials would be carried out. For validity of the experiments, duplication of the experiments would also be carried out in the same sequential manner.

3.2   Single Grit Tests

For the SG test [3] a piece of SG was glued into a microscopic drilled hole of the specially designed steel plate. The same conditions for these tests were the same as those discussed in previous SG work [3].

Pencil break tests [18-19] displayed a large response time to what can only be described as a microsecond fracture [3]. In addition the SG tests which are significant when displaying the energy intensities against that of the known force phenomenon (including the material interaction) also displayed the same phenomenon. This is attributed to the memory effect and reflections of the micro fracture where the signal is prolonged in terms of duration. Due to this memory effect in previous work [3] it was noticed that rubbing was classified on the grit exit and this was significant to rubbing with slight plastic deformation where the signal oscillations were tending towards the steady state and therefore similar to the rubbing signals. Here another condition should be identified such as rubbing with slight plastic deformation.

Table 1 displays the material characteristics of the two tested aerospace materials.

Table 1 displays aerospace material properties used in this work [23]

3.3   Acoustic Emission Statistical Tests

This section looks at statistical and regression analysis to verify the suitability of the various forms of AE when exerted to different prolonged stresses.

Figure 3 Single Grit Tests with acoustic emission and force

Figure 3 displays the AE SG tests which were correlated with force measurements (prolonged stress initiated at the same distance). Due to difficulties in obtaining force measurements for SG tests [3], the test set displayed by Figure 3 is small however general trends can be observed. With respect to these tests it can be seen that as the force increases so does the AE voltage amplitude.

4. Acoustic Emission Digitised Signal Analysis

4.1 Single Grit Tests for CMSX4

In research displayed in work [23] both the AE time extracted signals and associated STFTs can be seen for rubbing, ploughing and cutting, where rubbing is significant of a recorded AE trace however with no physical scratch mark present. Figure 4 displays the STFT with much greater intensities and higher frequencies when the cutting phenomenon takes place however just before and after this phenomenon lower intensities with lower frequency components are recorded this is known as the ploughing phenomenon. Figure 4 is displayed here reference to previous work [23] and acts as a comparison between SG and MG: grinding and grinding burn.

As the AE energies are based on relative reference quantities of the raw extracted AE time signal, force is also correlated against the phenomena to give more absolute quantities for comparison. In short, the voltage amplitudes of SG were correlated to a recorded force for SG experiments (see Figure 3 for more information).

Figure 4 SG1 Test 2 Hit 6 displays the STFT of both cutting and ploughing phenomena for CMSX4

In achieving the force measurements, problems were noticed when trying to obtain the ploughing forces before and after the max cutting force was detected. Looking at previous work [23] it can be seen that the rubbing phenomenon occupies very low frequency components with low, associated amplitudes where Figure 4 displays a shift to higher frequency components with higher associated amplitudes when approaching cutting. Looking towards the right of Figure 4 these signals are more significant of the ploughing phenomenon where less material penetration is occurring and more energy is dispersing laterally across the workpiece.

4.2   Single Grit Tests for Titanium-64

To see the general effects a second similar aerospace material was selected: Titanium-64 (see Table 1). The same tests as displayed in the Section 4.1 are repeated here to see the change in frequency band domination and, their respective intensities. The images of AE time extracted and rubbing STFT images can be found in [23] also.

Figure 5 AE STFT SG2 Test 2 Hit 6 of Cutting/Ploughing phenomenon for Titanium-64 material

In comparison between the two materials there appears to be similar levels of intensities for the said phenomena which is significant to the same applied stresses however the emitted spectrum of the recorded AE signal for Titanium-64 has much higher frequency components when compared to that of CMSX4. This can be attributed to three factors: Titanium-64 is a much more combustible material with a lower coefficient of thermal conductivity and lower hardness when compared to

CMSX4 (see Table 1). The emitted AE can therefore vibrate more, significant to less material damping (note slightly more material is removed due to the lower material resistance). Such assumptions are further amplified when looking at Figure 5 where greater intensities are found due to the cutting and ploughing material removal mechanisms also correlated to slightly higher DOC (same setup for both material trials using an A55 machine centre with 1 µm increments).

Therefore it is expected that Figure 5 has higher intensities due to a measured slightly higher DOC, when compared to Figure 4. With similar setups, the time signals give good correlation to similar emitted AE signals for both materials. Another assumption is based on the material hardness (see Table 1) where the lower recorded DOC of CMSX4 is also associated with higher material hardness value which is significant to greater resistance when compared with Titanium 64.

The work investigating SG scratches correlates well to current work made by Opoz and Chen [24] where the results presented here are more concerned with the energies of AE and in [24] more concerned with the grit wear and SG scratch mechanics. It was noticed that the measured force amounts in this work are higher than what was detected in [24] this is due to [24] investigating micro grinding mechanisms with a smaller diameter wheel, different material hardness (EN24), diamond cutter as opposed to Al_2O_3 and, grit size was also considered much smaller in terms of the contact area. The work correlates well where the lower energies are found at the beginning of the grit scratch interaction which is significant to rubbing (the majority of rubbing signals was found in the penultimate grinding pass where only elastic phenomenon was identified on the surface). After rubbing the intensities start to

increase, this is significant to ploughing where the depth of cut is less than 0.5 µm, immediately after, the higher intensities are found which is indicative of cutting. After cutting, towards the end of the scratch the grit phenomena tends back towards ploughing and again at the final exit point: rubbing with slight plastic deformation. This final grit phenomenon can be a problem for classification systems [3], [23] where the AE memory effect and time-frequency translation can result in the detection of rubbing where instead a fourth phenomenon should be considered namely: rubbing with slight plastic deformation. Note the varying force intensities of [24] for cutting, ploughing and rubbing correlate well with work here in terms of both extracted force signals and that of acoustic emission.

4.3   Burn Tests for CMSX4 and Titanium-64 materials

In correlating the SG phenomena with MG grinding phenomena of burn the following figures display AE signals for the same materials Figures 6(a) and 6(b): CMSX4 no/burn respectively and Figures 6(c) and 6(d): Titanium-64 no/burn respectively. Similar to sections 4.1 and 4.2, force is also correlated with the recorded AE events to give more absolute energy references (see Figure 7 and Table 2).

Figure 6 Top: (a) No Burn and (b) Burn for CMSX4 Bottom: (c) No Burn and (d) Burn for Titanium-64

Figures 6 and 7 display the respective time and time-frequency spectra for the said macro grinding phenomenon: burn. Not surprisingly by the energy maps of Figure 7 are somewhat similar when comparing the two materials no burn and burn phenomenon (CMSX4: Figures 7(a) and 7(b) and Titanium-64: Figures 7(c) and 7(d)) this is due to the same machining conditions (see machining parameters below

Figures 6 and 7). The burn recorded force signals were found towards the end of each signal, looking at Figure 7 in greater depth toward the end of each signal there is a rectangular distribution of high intensities just before and at this point this is significant of burn phenomenon (in the titanium case: severe burn see Figures 6(d) and 7(d)). At the beginning of the signals the opposite is true where no burn was observed.

Figure 7 Top: STFT for (a) No Burn and (b) Burn for CMSX4 and Bottom: STFT for (c) No Burn and (d) Burn for Titanium-64

Table 2 Burn force results for selective comparison tests

Table 2 displays the selected force recorded results correlated to the repetitive AE events of Figures 6 and 7. In the following sections the AE signals are compared with sliced STFT amounts correlated to the specific physical material phenomenon – these slices of the STFT relate to the FFT of a particular time interval reference to the total STFT plot. Such dominant energy quantities were used to correlate the micro with macro phenomena events using transparent classification techniques such as classification regression trees (CART). The respective dB values were not normalised and instead left to ensure good demarcation between the different micro and macro phenomena. Figure 8 displays the burn results for test 4 along with a loaded wheel from increased heat due to friction and ploughing phenomenon (promoting burn through lower dressing ratios).

Figure 8 left: Recorded Surface for Titanium-64 and right grinding wheel loading (Test 4)

5.   Transparent Classification technologies

The treeviewer classifier uses the CART algorithm to carry out classification, CART is particularly useful in segregating n-dimensional data sets and produces transparent, easily readable, classification rules. There are other techniques which are similar to Optimised Fuzzy Clustering such as Genetic Programing (GP) as seen in work discussed by Griffin and Chen, [2], however when faced with n-dimensional data with no pre-processing reduction, other techniques are more favourable such as CART.

CART builds classification and regression trees for predicting continuous dependent variables (regression) and categorical predictor variables (classification) [21].

It achieves its functionality by recursively splitting the feature space into sets of non-overlapping regions and, by predicting the most likely value of the dependent variable with each region. It generates a binary tree through recursive partitioning, where it splits the data into sub-nodes based on the minimisation of a heterogeneity criterion computed at the resulting sub-nodes. With the CART algorithm, the tree is forwardly propagated, using forward stepwise regression, for best purity of node split. The best node split becomes the chosen value of partition (for a good splitting criteria see Eq. 1).

$$PRE = \Phi(s, t), \tag{1}$$

where PRE is the minimum production reduction error and s is the split at any node t. The best purity measure looks at the best unique minimal classification where

impure would be to have many unnecessary classes. For the CART algorithm the accuracy percentage of classification is used as the best purity measure.

This method of classification is chosen because the tree fitting methods are actually closely related to cluster analysis [25]. This is where each node can be thought as a cluster of objects, or cases, that are split by further branches in the tree. Note that the top node covers the whole sample set and each remaining node contains a subset of the original sample, and so on as the split level increases [25].

6. Classification Results

The following section looks at the CART classifications of SG and MG grinding/burn tests respectively which aims to show the similarities of energy quantities in terms of intensities and frequency distribution connecting micro with macro phenomena material events.

6.1 Single Grit Tests for CMSX4 and Titanium-64 materials

Parallel coordinates is a statistical method that is used to display the signal frequencies of interest. To allow a more focused appreciation it was observed that no significant signal phenomena existed beyond 500 kHz and therefore only the bandwidth between 80 kHz to 500 kHz is represented in the parallel co-ordinate figures.

Figure 9 parallel coordinates of AE signals in terms of cutting, ploughing and rubbing phenomena: CMSX4 material

Figure 9 displays the three phenomena broken up into cutting (red), ploughing (blue) and rubbing (green) where the lowest intensities and frequency components are associated with rubbing then ploughing which occupies similar frequency bands to that of cutting however with much lower intensities. Significantly cutting has higher amplitudes in the 90 kHz, 135 kHz, 200 kHz, 250 kHz and 400 kHz bands when compared with ploughing.

Figure 10 Output CART Tree for cutting, ploughing and rubbing phenomena: CMSX4 material

Looking at the classification given by CART of Figure 10 rubbing is much easier to segregate than the other two phenomena which are similar in nature albeit with subtle amplitude differences. The nodal split decision points of x18, x27 and x40 all correlate to the frequency bands: 90 kHz, 135 kHz and 200 kHz respectively, which are classed as significant for the CMSX4 cutting phenomenon. Similar to Figure 9 the three phenomena are broken up into their relevant segments. The lowest intensities and frequency components are again associated with rubbing then ploughing and finally, cutting. Significantly cutting has higher amplitudes in the, 100 kHz, 140 kHz, 225 kHz, 250 kHz, 290 kHz and 465 kHz bands when compared with ploughing.

Figure 11: parallel coordinates of AE signals in terms of cutting, ploughing and rubbing phenomena: Titanium-64 material

Both Figures 9 and 11 displays the salient frequency components for SG material mechanisms for the two materials: CMSX4 and Titanium-64 respectively. The energy intensities are labelled with the respective dB levels and energy gains. Note also the Signal to Noise ratios can be used to link the AE phenomena from SG to the macro

grinding event where the noise levels for SG was -2.01 dB. Such levels can be used for automated signal recognition of differing material conditions for example cutting is related to a specific range of dB when compared with both ploughing and rubbing (such level identification can be easily adopted in fast reactive real-time monitoring systems). However for more accuracy and a more dynamic picture STFTs are used giving higher fidelity with frequency components.

The CART classification for Titanium-64 SG tests are similar to the CART classification displayed by CMSX4 tests (Figure 10) where all 3 phenomena were segregated. The nodal split decision points of 93 correlate with the frequency band: 465 kHz, which is significant for Titanium-64 cutting phenomenon (See Section 4.1). For both SG classifications CART trees were found for the same classifications albeit with the added output parameter of force. Such tree outputs were considered too complex to display and instead a max/min table of associated forces can be found in Table 3. It can be seen that the dominant cutting frequency bands are higher than that of CMSX4 this is due to a lower hardness value with less material resistance, not to mention it is a more combustible material.

Table 3 Min and Max recorded forces for SG experiments

Table 4 displays the classification accuracy of unseen test data applied to the CART trees for test validation [3].

Table 4 SG CART Classification results

6.2   Burn Tests for CMSX4 and Titanium-64 materials

This section discusses the parallel coordinates and CART classifications for grinding/grinding burn of both CMSX4 and Titanium-64 materials. Figure 12 displays the significant frequency bands and their associated intensities through using parallel co-ordinates. The following bands are displayed as significant in terms of intensities segregating CMSX4 burn from no burn: 115 kHz, 130 kHz and 160 kHz.

Figure 12 parallel coordinates of AE signals in terms of burn and no burn phenomena: CMSX4 material

Figure 13: Optimised CART Rules for burn and no burn – CMSX-4 material

Similar to Figures 9 and 11, Figure 12 displays the dB signal amounts where grinding noise was identified as 17 dB (both material tests). For CMSX4 material, 140 kHz, 160 kHz and 360 kHz are the differentiators between burn and no burn where the burn intensities are much higher.

Comparing the CART classifications of Figure 13 with the parallel coordinates of Figure 12, the nodal tree discriminators find the following nodes significant in terms classifying the AE time-frequency signal: x23, x26, x30 and x32 which relate to the following frequency bands: 115 kHz, 130 kHz, 150 kHz and 160 kHz respectively, and are very similar to the dominate frequency bands displayed by Figure 12. In comparing the CMSX4 SG with burn tests the similarities are found at the 135 kHz frequency band where the amplitude is 17.5 dB for SG compared to 34 dB for burn (max SG peak compared to the corresponding peak in burn). The force amounts for the CMSX4 SG and burn tests are 35N and 1500N respectively which equates to nearly 42 times compared to that of AE with 53 times. It was noticed the dominant frequency bands of SG are somewhat similar to those of the burn cases. With CMSX4

there is a greater thermal and, plastic deformation resistance and for this reason the level of burn was slight (25%) in comparison with Titanium-64 which was identified as much greater with 70% total workpiece burn.

Figure 14: parallel coordinates of AE signals in terms of burn and no burn phenomena: Titanium-64 material

Comparing the CART classifications of Titanium-64 with the parallel coordinates of Figure 14, the nodal tree discriminators find the following nodes significant in terms classifying the AE time-frequency signal: x23, x25, x33 and x85 which relate to the following dominating frequencies: 115 kHz, 125 kHz, 165 kHz and 425 kHz and are very similar to the dominate frequencies displayed by the Titanium-64 CART classifications.

In comparing the Titanium-64 SG with burn tests the similarities are found at the 115 kHz, 165 kHz frequencies where the amplitude is 6.02 dB for SG compared to 49.5 dB for burn with the addition of the higher orders of frequency occupying 425 kHz with an amplitude of 19.1 dB for SG compared to 34 dB with burn. The maximum force amounts for the Titanium-64 SG and burn tests were 40N and 1900N respectively which equates to nearly 47 times more compared to that of the AE (dominate SG band vs. corresponding burn band: 44 times). Similarly the dominant frequency bands of SG are somewhat similar to those of the burn cases. As the Titanium-64 endured significantly more burn (due to its low thermal conductivity) this can be seen with the higher frequency components around the 400 kHz range which correlates with previous work [2], [8], [13]. In addition, it should be noted that all burn cases have higher intensities from 100 kHz to 500 kHz bands compared to normal grinding which is significant in high % burn cases. Comparing the dominate

burn frequency bands with their corresponding SG frequency bands the levels are 46 dB and 16.7 dB for CMSX4 and 49.5 dB and 10 dB for Titanium-64. A Simulink model was created to work out the specific and cutting energy of both SG and MG grinding mechanisms. The width of SG was measured as 300 µm and for the MG: 15 mm and the calculated power was 24939 times more for MG than SG which is significant to the differences in volume of DOC and width. When comparing the same width (AE sensor only conveys 2D information) with different DOC (SG and MG) the difference is 498 times. Note the displayed AE energies are stationary peak comparisons and not an accumulation of energies. Looking at Figures 9, 11, 12 and 14, if accumulation of energy peaks were made, similar differences would also be found.

The idea is to understand the energy pattern at the unit SG level and build up to the total grinding wheel area to give the grinding perspective. The method of the parallel coordinates and CART rules ensure a link between SG and MG phenomena.

Table 5 confirms the accuracy of the burn classifications for each material. Such test data is based on unseen data testing the classifiers ability to generalise rather than just fit the data. For both materials, the force and burn tests are high in accuracy giving further confidence.

Table 5 Burn CART classifications results

8. Conclusions

The experiments discussed within this paper were designed to investigate the correlations of AE and force based on the measured AE event. Such experimental tests displayed similar frequency band occupation of both SG and burn tests albeit the intensity levels were much higher in the case of grinding/burn. This work looks to connect previous SG work with the MG phenomena in terms of grinding/burn.

For a model investigating dominate energy bands essentially the same frequency bands of the SG tests are occupied for the MG tests albeit the intensities are much higher in the burn case. Another observation was the respective frequency bands from the burn tests were slightly higher up the frequency spectrum than their SG counterparts, this shift is attributed to the burn phenomenon emitting more heat and mechanical energy as opposed to just mechanical energy. Such changing intensities can be quantified in terms of the micron event to the grinding/burn event giving more control in identifying the onset of unwanted anomalies. The parallel co-ordinates and CART classifications were significant in displaying the connections between micro and macro events.

No work before has looked at correlating the SG event with the MG event using AE energies, specifically with the burn phenomenon. This work is especially important for the modelling of grinding technologies based on their emitted energies when in contact with a specific material. Lastly, there was a lot more burn obtained during the Titanium-64 (due to low thermal conductivity) tests when compared with CMSX4 where such identification can be found when comparing the low frequency band utilisation with 50% more intensity in amplitude.

References

[1] Royer, D., and Dieulesaint, E. (2000). Elastic Waves in Solids I, II. New York, Springer-Verlag Berlin Heidelberg.

[2] Griffin J and Chen X, (2009), Multiple Classification of the Acoustic Emission Signals Extracted During Burn and Chatter Anomalies Using Genetic Programming, International Journal of Advanced Manufacturing Technology, 45 (11-12) 1152-1168.

[3] Griffin, J. (2014), Traceability of Acoustic Emission measurements for a proposed calibration Method – Classification of Characteristics and Identification using signal analysis, Mech.Syst.SignalProcess,

[4] Chen, X., Griffin, J., and, Liu, Q., (2007), "Mechanical and Thermal Behaviours of Grinding Acoustic Emission, International Journal of Manufacturing Technology and Management (IJMTM), Vol. 12, No. 1~3, pp. 184-199."

[5] Coman, R., Marinescu, I. D., (1999) Acoustic emission signal - an effective tool for monitoring the grinding process, Abrasives Dec/Jan: 5.

[6] Webster, J., Marinescu and I. Bennett, R., (1994) Acoustic emission for process control and monitoring of surface integrity during grinding, Annals of CIRP, 43(1), 299-304.

[7] Chen, M. Xue, B. Y. (1999). Study on acoustic emission in the grinding process automation. American Society of Mechanical Engineers, Manufacturing Engineering Division, MED Manufacturing Science and Engineering - 1999 (The ASME International Mechanical Engineering Congress and Exhibition), Nov 14-Nov 19 1999, Nashville, TN, USA, ASME, Fairfield, NJ, USA.

[8] Aguiar, P. R.; Willet, P. & Webster, J. (1999). Acoustic emission applied to detect workpiece burn during grinding, In: Acoustic emission: Standards and Technology Update, ASTM STP 1353, S. J. Vahaviolos, (Ed.), 107-124, American Society for Testing and Materials, West Conshohocken, Pennsylvania, USA.

[9] Subhash, G., Loukus J.E., and Pandit S.M., (2001), Application of data dependent systems approach for evaluation of fracture modes during single-grit scratching, Mechanics of Materials 34, pp 25-42

[10] Wang, H., and Subhash, G., (2002), An approximate upper bound approach for single-grit rotating scratch with a conical tool on pure metal, Wear 252, pp. 911-933

[11] Liu, Q., Chen X., and Gindy N., (2005). "Fuzzy pattern recognition of AE signals for grinding burn." International Journal of Machine Tools & Manufacture 45(7-8): 811-818.

[12] Aircraft Accident Report--United Airlines Flight 232, McDonnell Douglas DC-10, Sioux Gateway Airport, Sioux City, Iowa, July 19, 1989, Report Number: NTSB/AAR-90106, 1990,

[13] Tonshoff, H. K. and K. T. Friemuth (2002). "Process monitoring in grinding." CIRP Annals - Manufacturing Technology 51(2): 551-571.

[14] Chen, X., W. B. Rowe, et al. (2000). "Analysis of the transitional temperature for tensile residual stress in grinding." Journal of Materials Processing Technology 107(1-3): 216-221.

[15] Chen, X. and Q. Liu (2004). "Grinding burn identification through AE monitoring." 3rd International Conference and Exhibition on Design and Manufacturing of Die and Moulds, ISAAT 2004.

[16] Ren Q., Balazinski M. Jemielniak K., Baron L. and Achiche S., (2013), Experimental and fuzzy modelling analysis on dynamic cutting force in micro milling, Soft Computing, 17, Pages 1687-1697.

[17] Ren Q., Balazinski M. and Baron L., (2012), Fuzzy Identification of Cutting Acoustic Emission with Extended Subtractive Cluster Analysis. Nonlinear Dynamics. 67(4), Pages 2599-2608.

[18] Boczar, T. and M. Lorenc (2006). "Time-frequency Analysis of the Calibrating Signal Generated in the Hsu-Nielsen System, Physics and Chemistry of Solid State."**7.3**: pp 585-588.

[19] Hatano, H., Chaya, T., Watanabe, S. and Jinbo, K. (1998). "Reciprocity Calibration of Impulse Responses of Acoustic Emission Transducers," IEEE Transations on Ultrasonics, Ferroelectronics, and Frequency Control, Vol. 45, No. 5[12], pp 1221-1228.

[20] Godin. N., Huguet. S., Gaertner and Salmon L., (2004), "Clustering of acoustic emission signals collected during tensile tests on unidirectional glass/polyester composite using supervised and unsupervised classifiers," NDT&E International 37, pp 253-264.

[21] Lawrence R.L. and Wright A., (2001), "Rule-Based Classification Systems Using Classification and Regression Tree (CART) Analysis," American Society for Photogrammetric engineering & remote sensing, pp 1137-1142.

[22] Kalpakjian, S. and Schmid, S.R., "Manufacturing Process for Engineering Materials", Prentice Hall, ISBN 0-13-040871-9, pp. 510-520, 2003.

[23] Griffin, J. and Chen X., (2014), Real-time Fuzzy-Clustering Classification of the characteristics of emitted Acoustic Emission during Horizontal Single Grit Scratch Tests, International Journal of Advanced Manufacturing Technology.

[24] Opoz T., and Chen X., (2012), Experimental investigation of material removal mechanism in single grit grinding, International journal of machine tools and manufacture, 63, pp 32-40.

[25] Coppersmith, D., S. J. Hong, and J. R. M. Hosking, 1999, "Partitioning Nominal Attributes in Decision Trees." Data Mining and Knowledge Discovery, Vol. 3, pp. 197–217.

Table 1 displays aerospace material properties used in this work [23]

Property	CMSX4	Titanium-64
Composition (WT%)	Mo: 0.6, Cr: 7, Ti: 1, Al: 5.6, Co: 10 Ni: 67, Re: 3, W: 6	C: 0.08, Al: 5.5-6.75, Fe: 0.30, H: 0.010
Density (kg/m^3)	8690	4650
Hardness	520HV	349HV
Tensile strength (MPa)	1090	950
Yield Strength (Mpa=N/mm^2)	990	880
Elastic Modulus (GPa)	18.5	109.6
Elongation (%)	10-12	14
Melting point (°C)	1395	1604
Passion's Ratio	0.273	0.34
Thermal Conductivity (W/mk)	12~63	6.70
Special heat capacity (K/kgK)	381~544	450
Thermal diffusivity (x10^{-6}m^2/s)	2.54~21	16

Table 2 Burn force results for selective comparison tests

TEST NUMBER	Force (N) Fy	Force (N) Fz	Burn (Y/N)
TEST 3	600	1700	N
TEST 4	700	1900	Y
TEST 7	560	1200	N
TEST 10	680	1500	Y

Table 3 Min and Max recorded forces for SG experiments

TYPE OF TEST	Min Force (N) CMSX4	Max Force (N) CMSX4	Min Force (N) Titanium-64	Max Force (N) Titanium-64
CUTTING	26	35	28	40

PLOUGHING	8	14	8	16
RUBBING	1	2	1	2

Table 4 SG CART Classification results

TYPE OF TEST	SG CPR CMSX4	SG CPR CMSX4	SG CPR Titanium-64	Force SG Titanium-64
CLASSIFICATION SCORES	96/100 = 96% 50% unseen cases	74/100 0 74%	118/126 = 94% 50% unseen cases	96/126 = 76%
% OF TEST DATA	26/26 cutting 48/52 ploughing 22/22 rubbing	19/26 cutting 40/52 ploughing 15/22 rubbing	20/23 cutting 53/58 ploughing 45/45 rubbing	19/23 cutting 40/58 ploughing 37/45 rubbing

Table 5 Burn CART classifications results

TYPE OF TEST	Burn CMSX4	Force CMSX4	Burn Titanium-64	Force Titanium-64
CLASSIFICATION SCORES	101/101 = 100%	187/201 = 93%	100/101 = 99%	190/201 = 95%
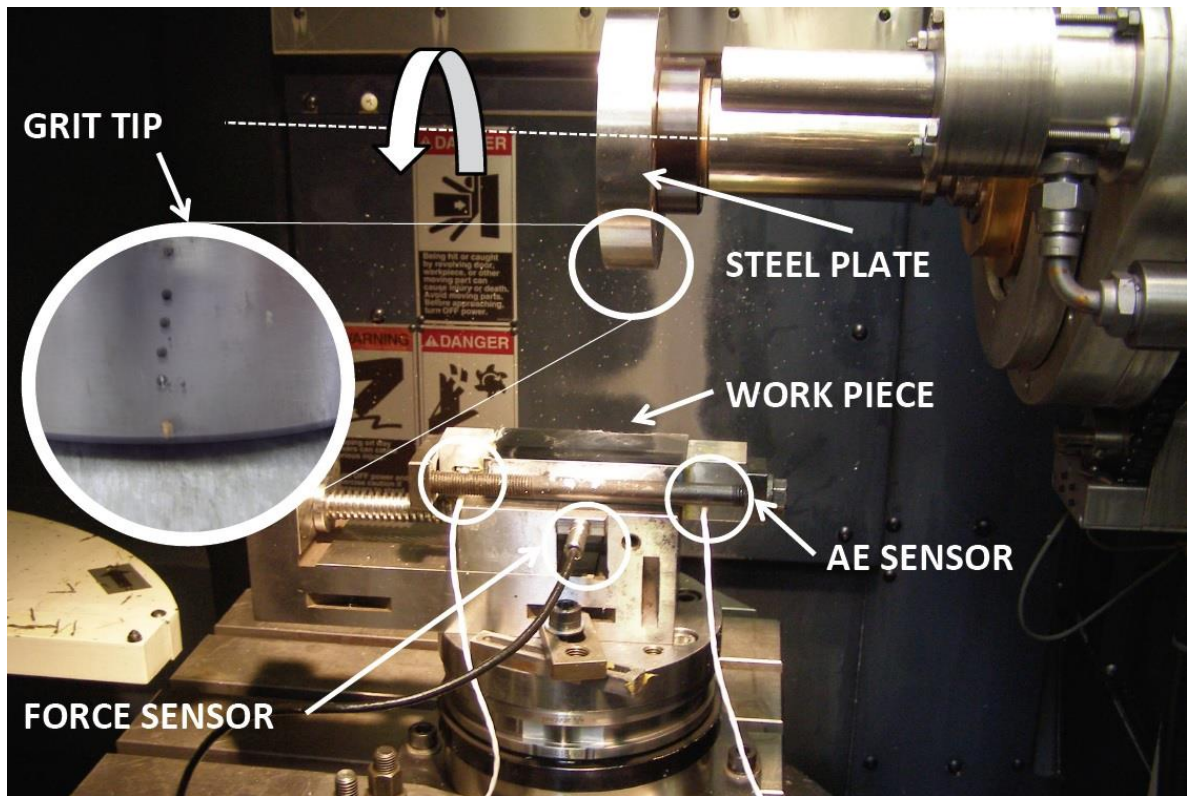
Figure 1 Single Grit Experimental setup
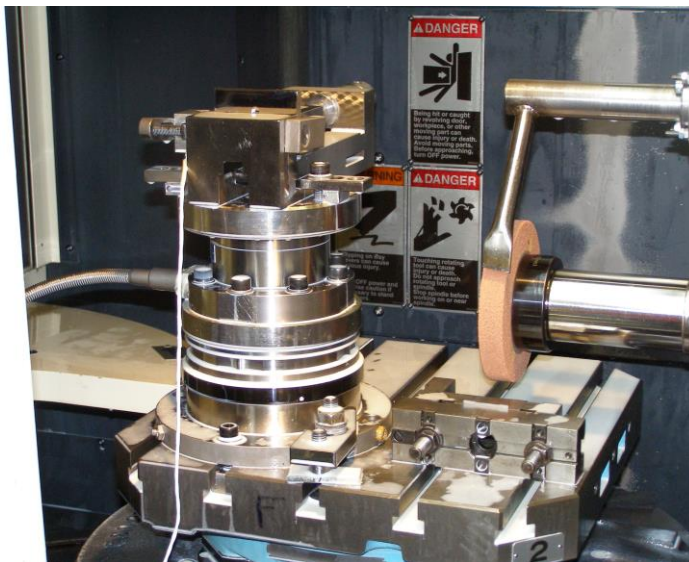
Figure 2 A55 Machine Centre Set-up for Burn Experiment (CMSX4)
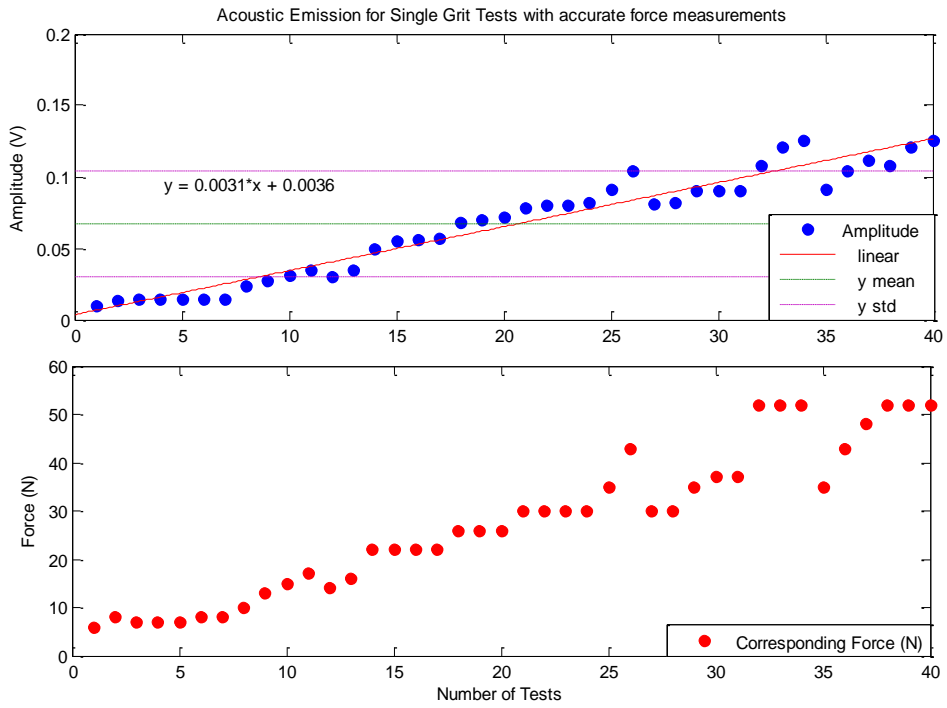
Figure 3 Single Grit Tests with acoustic emission and force
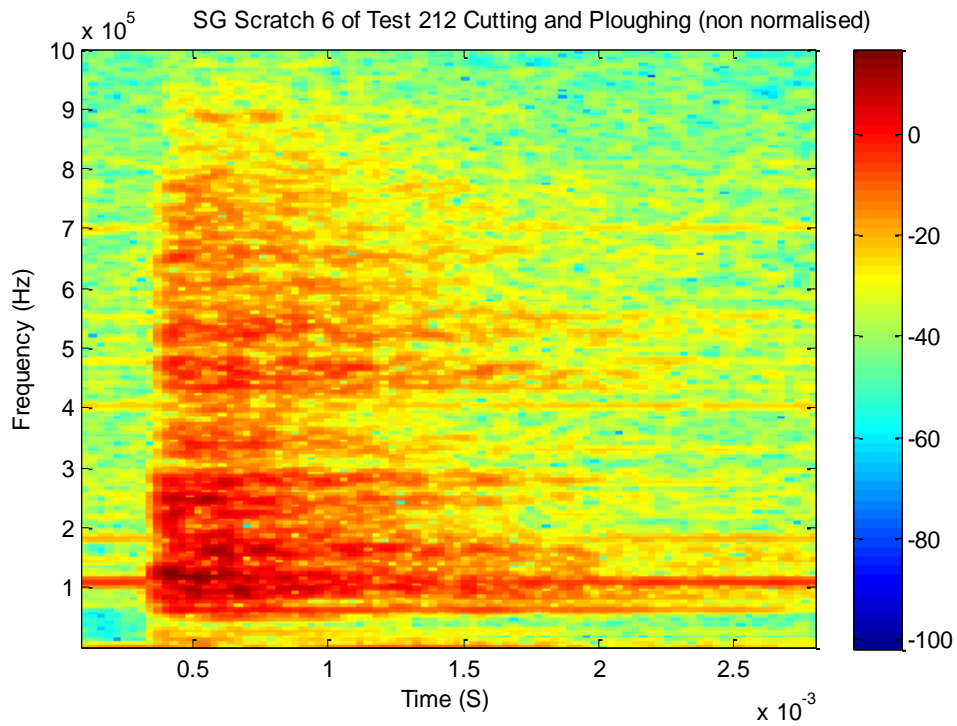
Figure 4 SG1 Test 2 Hit 6 displays the STFT of both cutting and ploughing phenomena
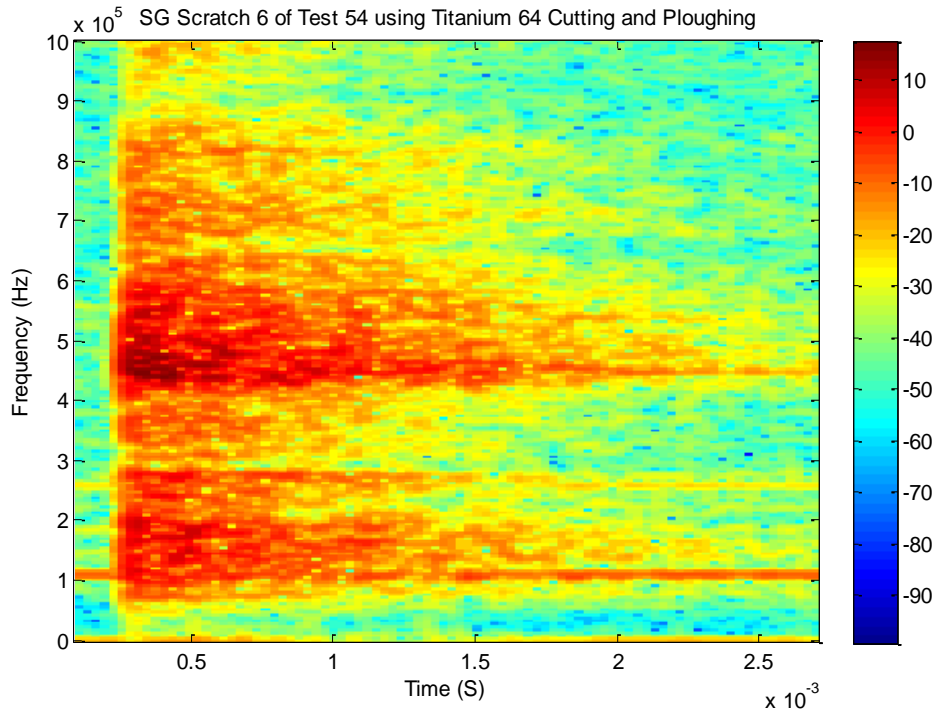
Figure 5 AE STFT SG2 Test 2 Hit 6 of Cutting/Ploughing phenomenon for Titanium-64 material
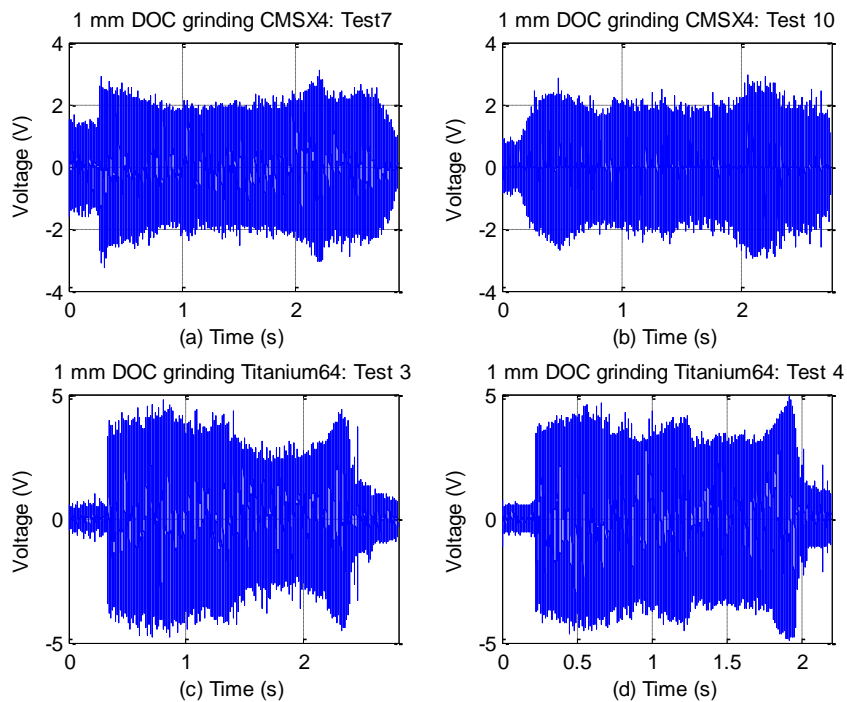
Machine: Makino A55; Grinding Wheel: Al_2O_3; Workpiece: CMSX4 and Titanium-64; Burn trials A_p 0.1mm $\rightarrow$ 0.6mm and 1mm, wheel thickness 15mm ; high pressure coolant for CMSX4 and Titanium-64: Vs= 35 m/s; Vw= 1000 mm/min (same conditions used for SG tests without coolant);

Figure 6 Top: No Burn and Burn for CMX4 Bottom: No Burn and Burn for Titanium-64
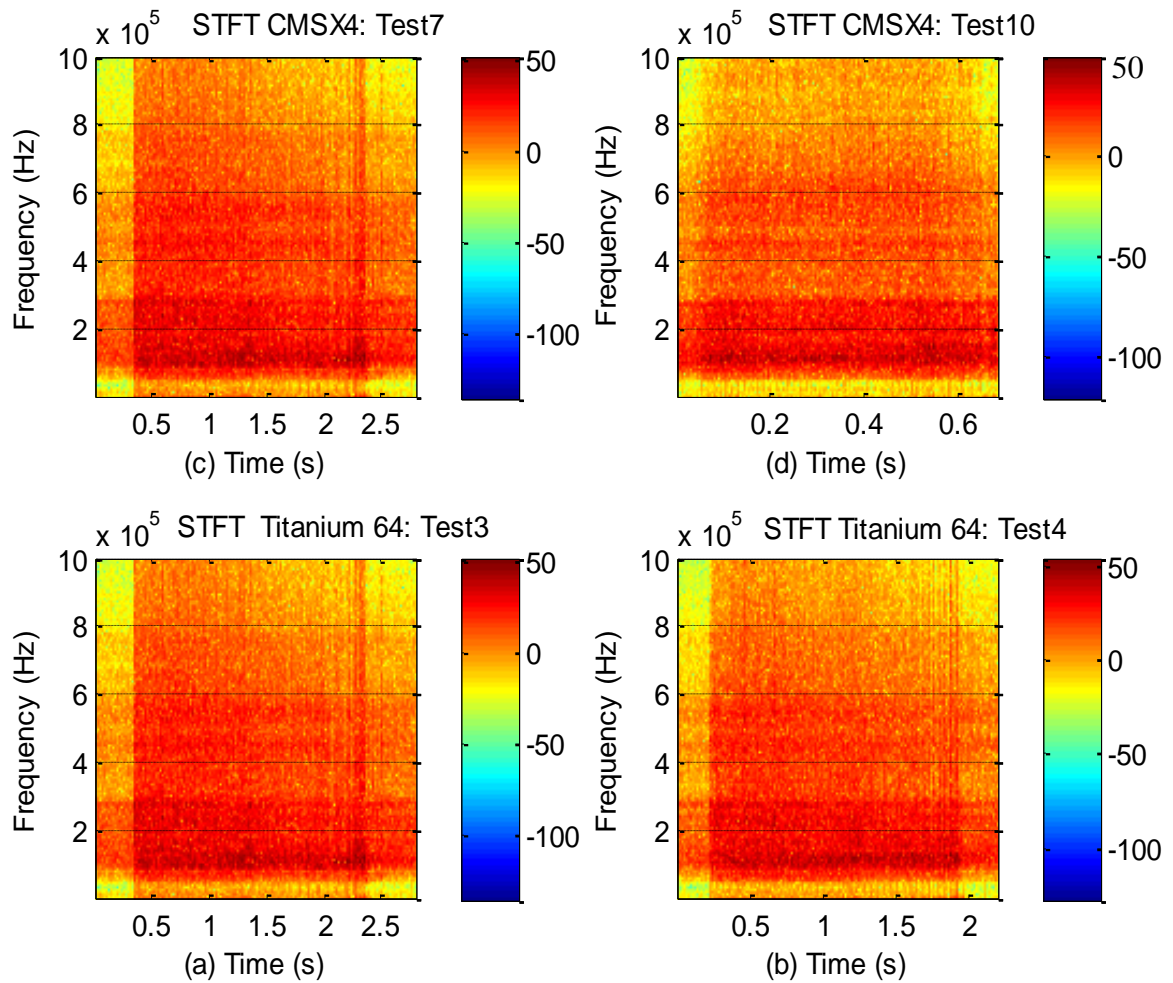
Machine: Makino A55; Grinding Wheel: Al$_2$O$_3$; Workpiece: CMSX4 and Titanium-64; Burn trials A$_p$ 0.1mm → 0.6mm and 1mm, wheel thickness 15mm ; high pressure coolant for CMSX4 and Titanium-64: Vs= 35 m/s; Vw= 1000 mm/min (same conditions used for SG tests without coolant);

Figure 7 Top: STFT for Burn and No Burn (CMSX4) and Bottom: STFT for Burn and No Burn (Titanium-64)
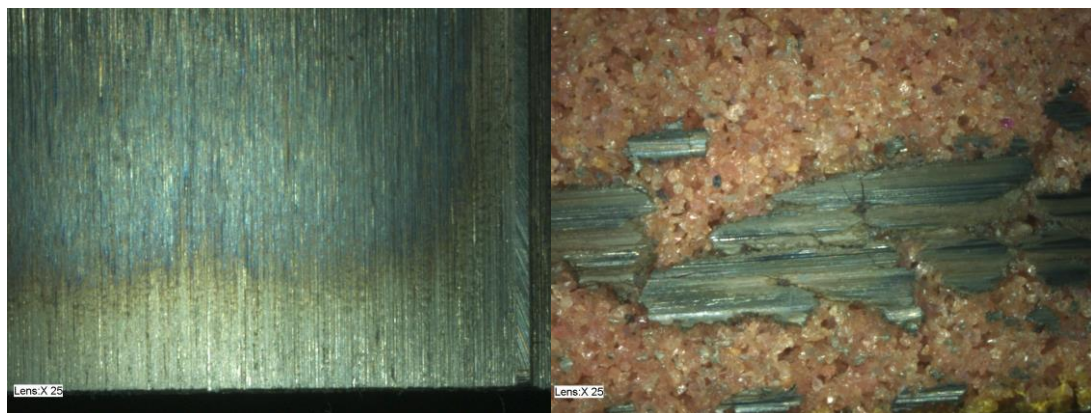
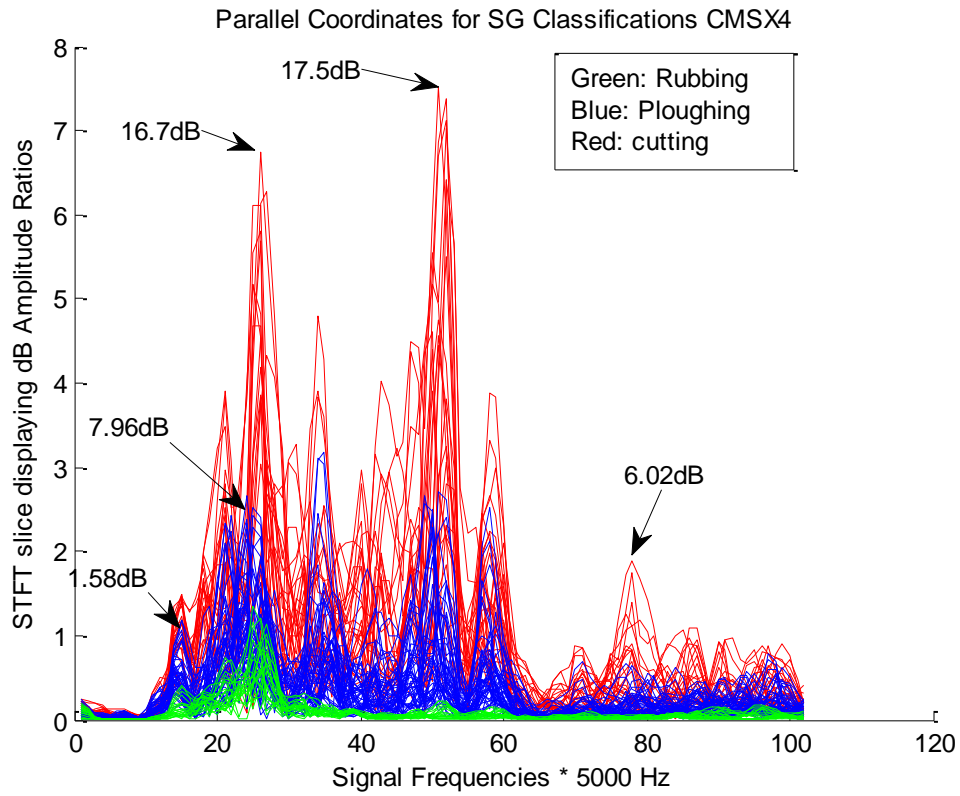Figure 8: left: Recorded Surface for Titanium-64 and right grinding wheel loading (Test 4)

Figure 9: parallel coordinates of AE signals in terms of cutting, ploughing and rubbing phenomena: CMSX4 material
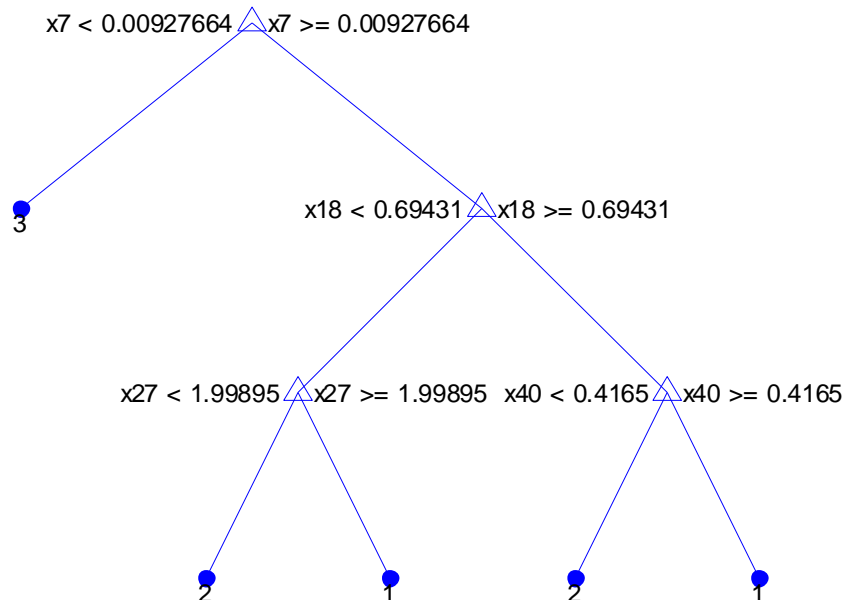
Figure 10: Output CART Tree for cutting, ploughing and rubbing phenomena: CMSX4 material
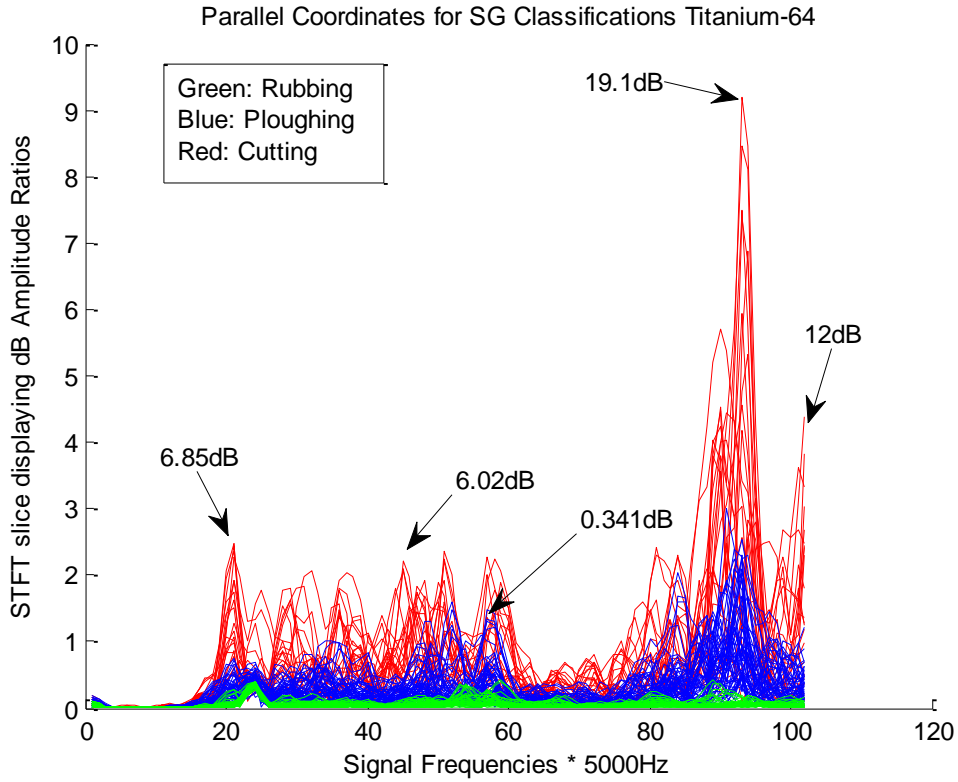
Figure 11: parallel coordinates of AE signals in terms of cutting, ploughing and rubbing phenomena: Titanium-64 material
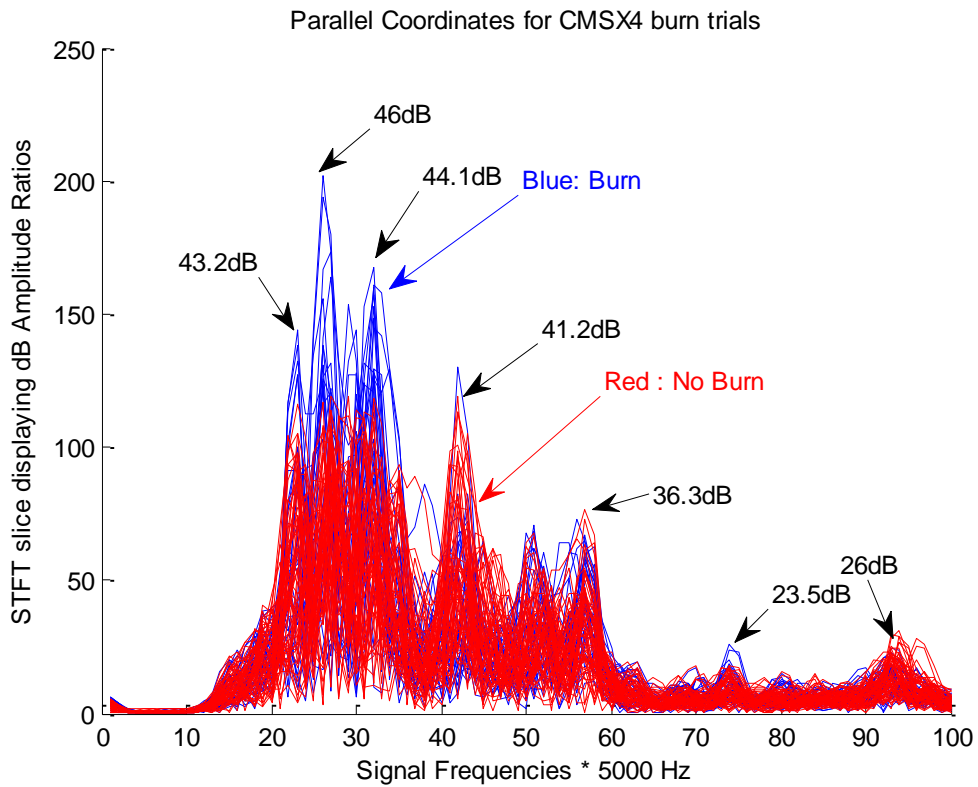

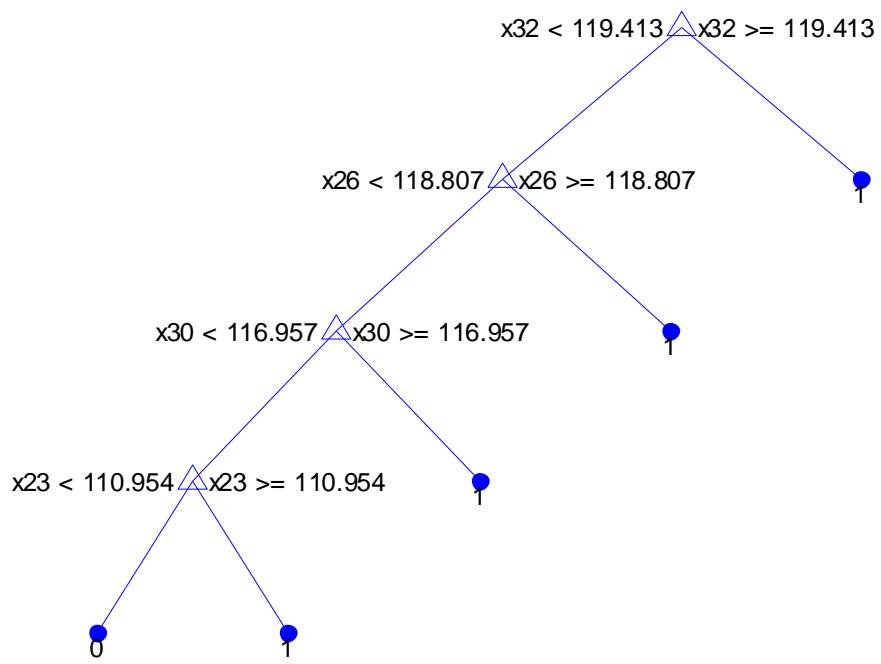Figure 12: parallel coordinates of AE signals in terms of burn and no burn phenomena: CMSX4 material

Figure 13: Optimised CART Rules for burn and no burn – CMSX4 material
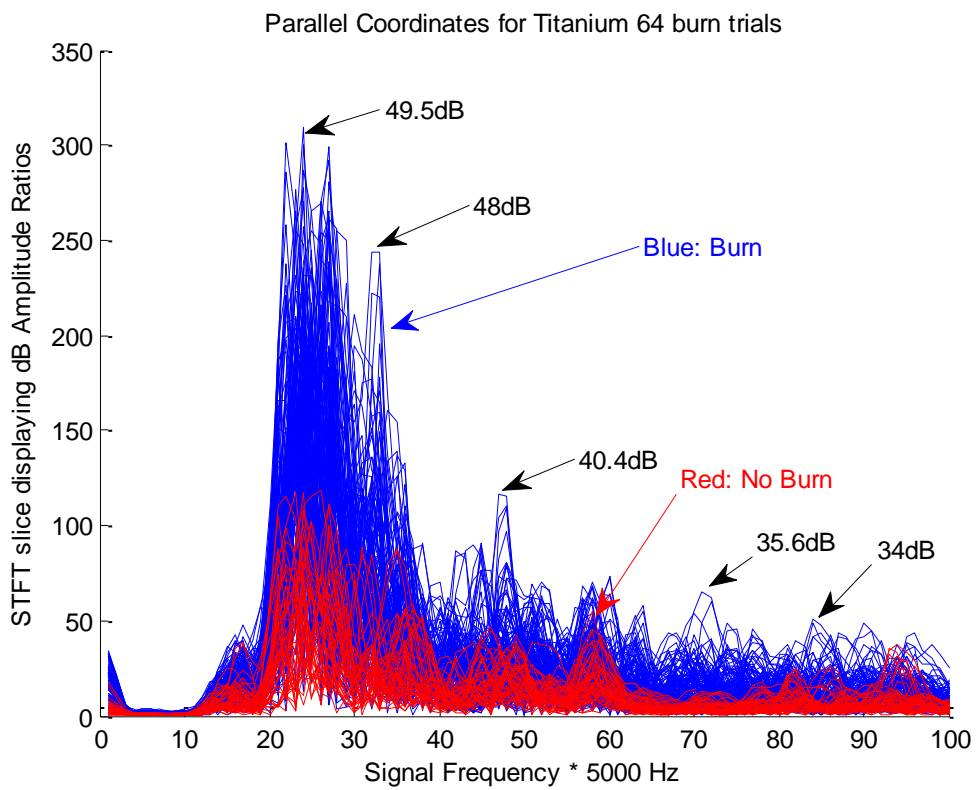

Figure 14: parallel coordinates of AE signals in terms of burn and no burn phenomena: Titanium-64 material